chemosensors

MDPI

Article

Adsorption Mechanism of SO_2 on Transition Metal (Pd, Pt, Au, Fe, Co and Mo)-Modified InP_3 Monolayer

Tianyu Hou [1], Wen Zeng [2,*] and Qu Zhou [1,*]

[1] College of Engineering and Technology, Southwest University, Chongqing 400715, China; houtianyu_luck@163.com
[2] College of Materials Science and Engineering, Chongqing University, Chongqing 400044, China
* Correspondence: wenzeng@cqu.edu.cn (W.Z.); zhouqu@swu.edu.cn (Q.Z.); Tel.: +86-130-683-05845 (Q.Z.)

Abstract: Using the first-principles theory, this study explored the electronic behavior and adsorption effect of SO_2 on an InP_3 monolayer doped with transition metal atoms (Pd, Pt, Au, Fe, Co and Mo). Through calculation and analysis, the optimum doping sites of TM dopants on the InP_3 monolayer were determined, and the adsorption processes of SO_2 by TM-InP_3 monolayers were simulated. In the adsorption process, all TM-InP_3 monolayers and SO_2 molecules were deformed to some extent. All adsorption was characterized as chemical adsorption, and SO_2 acted as an electron acceptor. Comparing E_{ad} and Q_t, the order of the SO_2 adsorption effect was Mo-InP_3 > Fe-InP_3 > Co-InP_3 > Pt-InP_3 > Pd-InP_3 > Au-InP_3. Except for the Au atom, the other five TM atoms as dopants all enhanced the adsorption effect of InP_3 monolayers for SO_2. Furthermore, the analysis of DCD and DOS further confirmed the above conclusions. Based on frontier orbital theory analysis, it is revealed that the adsorption of SO_2 reduces the conductivity of TM-InP_3 monolayers to different degrees, and it is concluded that Pd-InP_3, Pt-InP_3, Fe-InP_3 and Mo-InP_3 monolayers have great potential in the application of SO_2 resistive gas sensors. This study provides a theoretical basis for further research on TM-InP_3 as a SO_2 sensor.

Keywords: InP_3 monolayer; transition metal doping; SO_2 sensors; DFT

check for updates

Citation: Hou, T.; Zeng, W.; Zhou, Q. Adsorption Mechanism of SO_2 on Transition Metal (Pd, Pt, Au, Fe, Co and Mo)-Modified InP_3 Monolayer. *Chemosensors* **2022**, *10*, 279. https://doi.org/10.3390/chemosensors10070279

Academic Editor: Simonetta Capone

Received: 1 June 2022
Accepted: 13 July 2022
Published: 14 July 2022

1. Introduction

Sulfur dioxide (SO_2) is a corrosive, toxic and colorless gas but has a strong pungent smell. SO_2 is mainly produced by the combustion of sulfur, which comes from the industrial production process and automobile exhaust emissions [1–4]. A low concentration of SO_2 gas has many negative effects on the human body, such as skin burns, the stimulation of cardiopulmonary function and respiratory inflammation. A high concentration of SO_2 gas can directly lead to human death. Sulfate aerosol generated by SO_2 oxidation in the atmosphere plays an essential part in the formation of $PM_{2.5}$, which is the chief culprit of smog weather. When SO_2 is dissolved in water, it forms sulfuric acid, which irritates the eyes and nasal mucosa [5–10]. SO_2 is closely associated with the formation of acid rain, which is one of the main air pollutants [11]. Therefore, the control of SO_2 concentration has aroused widespread concern, and it is particularly important to develop a gas sensor with high sensitivity to monitor SO_2.

In recent years, the discovery and preparation of graphene has triggered a wave of scholars' research on two-dimensional (2D) materials. However, the zero-band-gap characteristic of graphene is an obstacle in some applications [12,13]. Therefore, in order to solve this problem, people have begun to explore new materials with better band-gap characteristics and graphene-like structures. Chemical sensors based on new 2D materials have been widely researched and applied in electrical equipment fault diagnosis and environmental gas monitoring, such as metal nitrides, transitional metal dichalcogenides, etc. [14–17]. New 2D materials containing main group III and V elements have become a hot

spot of research attention since the appearance of black phosphene materials [18,19]. The structural and bonding properties of novel 2D monolayers contained In sheet systems (such as InO and In_2O_3) have been researched by employing DFT, and they have been successfully synthesized [20,21]. The InP_3 monolayer is a new layered semiconductor material with a honeycomb structure. According to Ouyang et al., the electronic conductivity and electronic thermal conductivity of the InP_3 monolayer show marked anisotropy. At room temperature, the average lattice thermal conductivity of the InP3 monolayer is about 0.63 W mK^{-1}, which is equivalent to that of classical thermoelectric materials [22]. Moreover, the InP_3 monolayer also has good optical properties, stable physical and chemical properties and high carrier mobility, which has great promise in the fields of battery materials, electronic/optical devices and gas sensors [23–26]. For example, Miao et al. found that the InP_3 monolayer shows semi-metallic and tunable magnetism in the case of hole doping, so it has a good application potential in electronic devices and photovoltaic devices [27]. Yi et al. proposed a new δ-InP_3 material and found that it has high carrier mobility and anisotropy. Through calculation, it was concluded that the δ-InP_3 monolayer is a N-based gas sensor with good reversibility and high selectivity and sensitivity [28]. Liao et al. investigated the adsorptive properties of Cr-InP_3 on H_2, C_2H_2 and CH_4 by density functional theory and discovered that Cr-InP_3 is a promising C_2H_4 sensor [29]. Therefore, the InP_3 monolayer is considered a base material for SO_2 adsorption.

As is well known, modifying and doping the base material with a transition metal (TM) can enhance electron mobility and promote the chemical activity of the base material, thus enhancing the gas adsorption capacity. The TM usually plays an essential role in improving the selectivity and sensitivity of nanomaterials to target gases [30–32]. In existing research, various doping atoms are used, but Pd, Pt, Au, Fe, Co and Mo as dopants have excellent doping and adsorption effects [33–38]. In our research, using density functional theory, we studied the electronic properties of an InP_3 monolayer doped with transition metals (Pd, Pt, Au, Fe, Co and Mo) and investigated the adsorption performance of SO_2 on the TM-modified InP_3 monolayer. The feasibilities of using TM-doped InP_3 monolayers as SO_2 gas sensors are proposed.

2. Computation Methods

In this study, the simulated computation was conducted in the $Dmol^3$ model of Materials Studio using the DFT method [39]. In order to obtain more reliable results, the Perdew–Burke–Ernzerhof (PBE) functional with high-precision generalized gradient approximation (GGA) was applied to calculate the electron exchange energy [40]. Tkatchenko and Scheffler's (TS) method was adopted to correct the weak van der Waals forces between the TM-InP_3 monolayer and SO_2. The DFT-D method can be employed to compute the weak interaction between the base material and the adsorbed atoms, which makes the results more accurate [41]. Double numerical plus polarization (DNP) was used as the linear combination method of atomic orbits. DFT semi-core pseudopotential (DSPP) was selected to deal with the correlated effects of TM atoms [42]. An InP_3 monomer with lattice parameters of 14.9 Å × 14.9 Å × 24.1 Å was constructed, and its vacuum layer thickness was set to 20 Å. In the geometric optimization, we used a Monkhorst-Pack grid k-point mesh of 12 × 12 × 1 for Brillouin zone integration [43,44]. Moreover, the maximum force and displacement values were selected as 0.002 Ha/Å and 0.005 Å, and the energy tolerance accuracy was set at 1×10^{-5} Ha. The self-consistent field tolerance (SCF) was 1×10^{-6} Ha to make the calculation results more reliable [45,46].

To ascertain the most stable structure of the system under different doping conditions, the binding (E_b) energy of each system is usually computed by the below formula [47]:

$$E_b = E_{TM-InP_3} - E_{InP_3} - E_{TM} \quad (1)$$

E_{TM-InP_3} and E_{InP_3} represent the energy of the TM-InP_3 monolayer and the energy of the InP_3 monolayer, and E_{TM} represents the energy of TM atoms [48].

Adsorption energy (E_{ad}) refers to the energy gained or lost by the system in the process of gas adsorption. It is an important indicator of adsorption difficulty. The calculation process is as follows [49]:

$$E_{ad} = E_{TM-InP_3/SO_2} - E_{TM-InP_3} - E_{SO_2} \quad (2)$$

where E_{TM-InP_3} and E_{SO_2} denote the energy of TM-InP_3 and SO_2, respectively. E_{TM-InP_3/SO_2} represents the energy of the TM-InP_3/SO_2 system. An E_{ad} less than 0 indicates that the adsorption process is exothermic, and if its absolute value is larger than 0.8 eV, it means that chemisorption occurs in the process [17,50].

Through Millikan population analysis, the charge transfer (Q_t) between the adsorbent surface and SO_2 can be known. The formula of Q_t is as follows [51]:

$$Q_t = Q_{after} - Q_{before} \quad (3)$$

Q_{before} and Q_{after} denote the charge of SO_2 before and after adsorption. Negative Q_t implies that electrons are transferred from the material to SO_2, and the adsorption material acts as an electron donor [52].

3. Results and Discussion

3.1. Structures of SO_2 and InP_3 Monolayer

The optimized SO_2 molecular model and its structural parameters are shown in Figure 1a. The SO_2 molecule has a symmetrical V-shaped structure, with the bond lengths of both S-O bonds being 1.480 Å and the bond angle of O-S-O being 120.031°. In this study, a two-dimensional InP_3 monolayer structure composed of 8 In atoms and 24 P atoms was adopted. Compared with an InP_3 multilayer system, a monolayer tends to have better semiconductor properties and carrier mobility. Its smaller band gap and better electrical conductivity are beneficial for its use as a gas sensing material. Therefore, in this work, the InP_3 monolayer was selected for doping and gas adsorption research [53–55]. The optimized InP_3 monolayer structure is shown in Figure 1b. Because the structure is symmetrical, there are two kinds of P atoms and two kinds of In atoms. In the InP_3 monolayer, the bond lengths of In-P and P-P are 2.531 Å and 2.236 Å, respectively, and the bond angles of P-In-P and P-P-P are 113.276° and 92.170°, respectively. The calculated energy band diagram of the InP_3 monolayer is shown in Figure 1c, and its band gap is 0.946 eV. The optimized structural data are in agreement with the data in References [43,56].

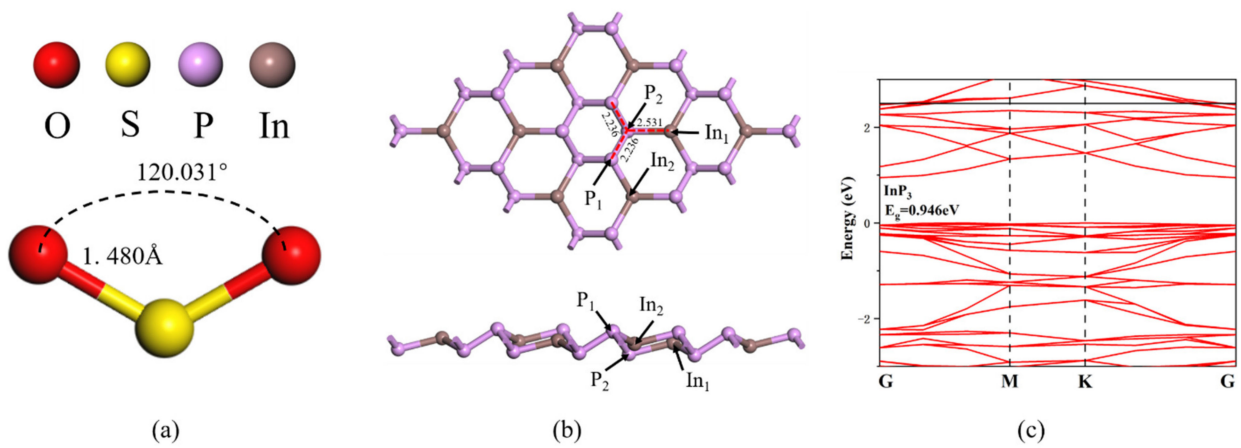

Figure 1. (**a**) Structure of SO_2 and (**b**) structure and (**c**) energy band of InP_3 monolayer.

3.2. Analysis of TM Atom (Pd, Pt, Au, Fe, Co and Mo)-Doped InP_3 Monolayer

In this study, TM atoms were used to replace the atoms in the InP_3 monolayer. According to the above analysis of the InP_3 monolayer structure, it can be known that its structure

has symmetry. As shown in Figure 1b, P_1, P_2, In_1 or In_2 can be used as modification sites. Models of TM atom doping in intrinsic InP_3 through the above four possible sites were constructed, and the models were geometrically optimized. The binding energy (E_b) of each doping mode can be calculated by Equation (1). Through the analysis of each structure, the optimal doping sites and the binding energy (E_b) are shown in Table 1. The doping models are shown in Figure 2.

Table 1. Optimum doping sites and binding energies of TM-doped InP_3.

	Pb-InP_3	**Pt-InP_3**	**Au-InP_3**	**Fe-InP_3**	**Co-InP_3**	**Mo-InP_3**
Doping Sites	P_1	P_1	P_2	P_1	P_1	P_1
E_b (eV)	−4.410	−6.393	−3.767	−4.806	−5.180	−5.670

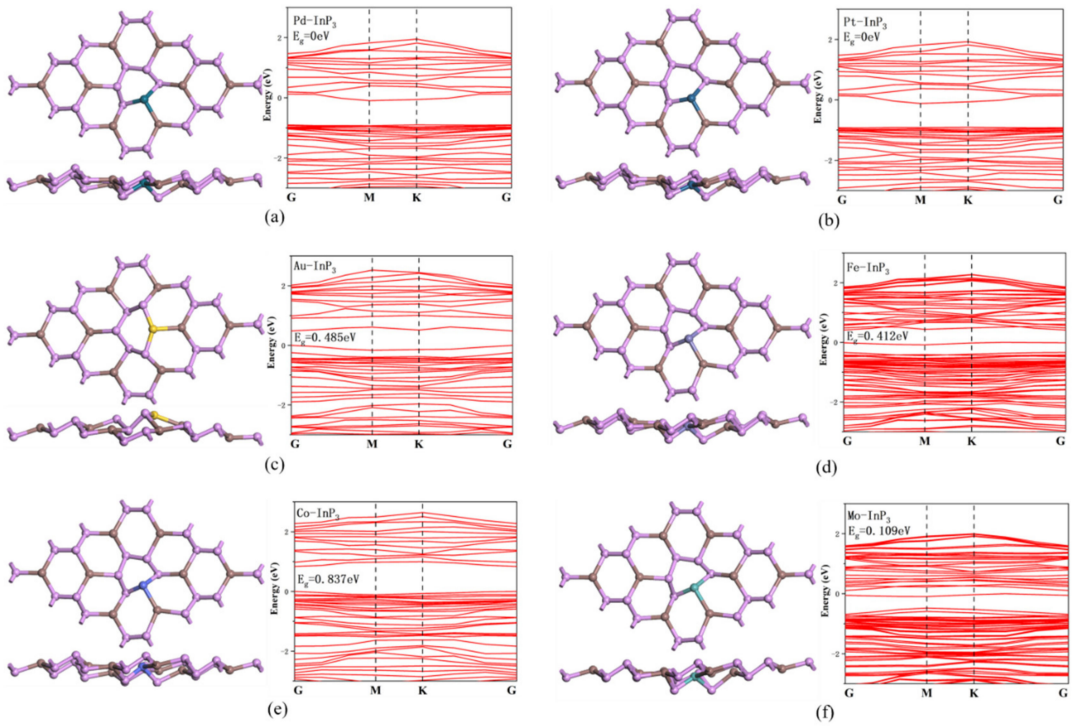

Figure 2. Structure and energy band of (**a**) Pd-InP_3, (**b**) Pt-InP_3, (**c**) Au-InP_3, (**d**) Fe-InP_3, (**e**) Co-InP_3 and (**f**) Mo-InP_3.

As can be observed in Table 1, the preferred doping sites of Pd, Pt, Fe, Co and Mo dopants are P_1 sites, while only the Au dopant is suitable for doping at the P_2 site. The E_b of the Pt-InP_3 monolayer is −6.393 eV, and the absolute value of E_b is the highest, while that of the Au-InP_3 monolayer is only −3.767 eV, and the absolute value of E_b is the lowest. The binding energies of the other four doping structures lie between those of Pt-InP_3 and Au-InP_3. This shows that the Pt dopant has the strongest binding ability with the InP_3 monolayer, and the doping structure is the most stable. On the contrary, the binding ability of Au to InP_3 is weak compared with the other five doping systems. It can be noted in Figure 2 that all six doping systems are deformed to some extent. By observing the energy band diagrams of the six systems, it can be found that, compared with intrinsic InP_3, the band gap of the InP_3 monolayer doped with metal atoms decreases from the initial 0.946 eV to 0 in Pb-InP_3, 0 in Pt-InP_3, 0.485 eV in Au-InP_3, 0.412 eV in Fe-InP_3, 0.837 eV in Co-InP_3 and 0.109 eV in Mo-InP_3. The reduction in the band gap means that electrons can easily complete the transfer from the valence band to the conduction band, which indicates that doping with the six metal atoms enhances the conductivity of the system. It is worth noting that after Pd and Pt dopants are doped into InP_3 monolayers, their band gaps are 0. This is

because Pd and Pt dopants induce the impurity state of the Pd-InP_3 monolayer and Pt-InP_3 monolayer, which results in strong N-type doping of InP_3. This behavior is similar to that of Au doping in the $MoTe_2$ system [57].

Figure 3 shows the density of states (TDOS and PDOS) of the six doping systems, which is used to analyze the electronic behavior of TM-InP_3 systems. Compared with the TDOS of intrinsic InP_3, the TDOS of the six TM-InP_3 systems all moved to low energy levels, which indicates that the conductivity of the six systems all increased, which is identical to the above conclusion of the energy band analysis. It can be found that the spin-down and spin-up of the TDOS of Fe-InP_3 and Mo-InP_3 systems are asymmetric, which indicates that the use of two dopants makes the InP_3 monolayer become magnetic. By analyzing the PDOS of the above two systems, it can be found that the Fe-3d orbit and Mo-4d orbit have high values near the Fermi level, which means that the electronic behaviors of Fe atoms and Mo atoms affect the magnetic transformation of the two systems. In TDOS, both Pd and Pt dopants contribute greatly to the TDOS at around −2.8 eV, and the value of the Au dopant is larger at around −3.5 eV. For Fe-InP_3, Co-InP_3 and Mo-InP_3 systems, the contributions of doped atoms to the TDOS of the system are mainly close to the Fermi level. In the PDOS diagram, the orbitals of the six doped atoms (Pd-3d, Pt-5d, Au-5d, Fe-3d, Co-3d and Mo-4d) markedly overlap with the In-5p and P-3p orbitals of InP_3, which implies that there are stable chemical bonds between TM atoms and InP_3 monolayers, and the overlap of Pt-InP_3 and Mo-InP_3 systems is the most pronounced. The above analysis shows that TM dopants can stably exist in InP_3 monolayers.

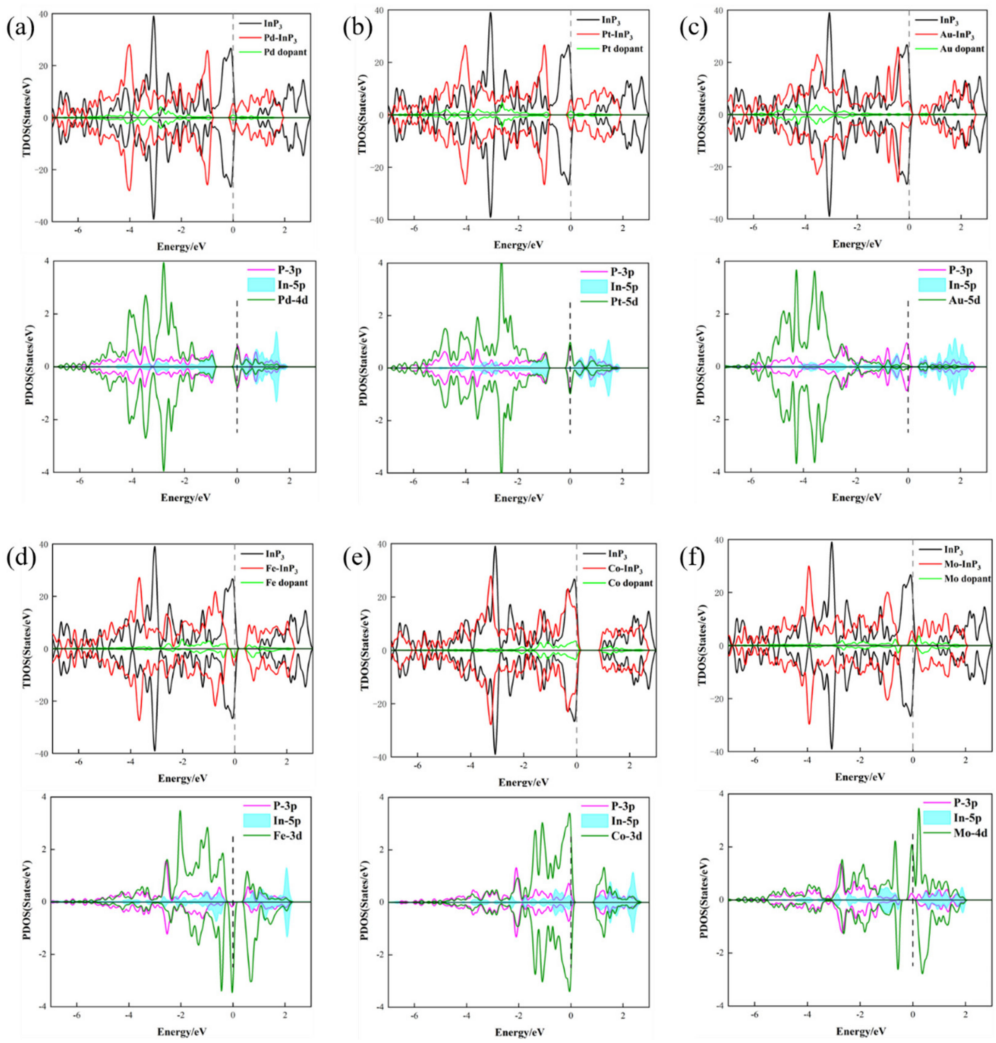

Figure 3. DOS of (**a**) Pd-InP_3, (**b**) Pt-InP_3, (**c**) Au-InP_3, (**d**) Fe-InP_3, (**e**) Co-InP_3 and (**f**) Mo-InP_3.

3.3. Analysis of Adsorption Behaviors of SO_2 on TM-InP_3 Monolayers

Next, the adsorption behaviors of SO_2 on TM-InP_3 monolayers were analyzed. The gas molecules approach the TM-InP_3 monolayer in different forms. After optimization, the adsorption energy (E_{ad}) was calculated by Equation (2), and the most stable adsorption structure was found. Table 2 presents the parameters and Millikan charge transfer of six optimal adsorption models. Figure 4 shows the optimized adsorption models and their deformation charge density (DCD). Table 3 lists the adsorption parameters of the intrinsic InP_3 monolayer for SO_2 (E_{ad} and Q_t in these data are derived from previous research results of Liao et al. [43]).

Table 2. Characteristic parameters of SO_2 adsorption on TM-InP_3 monolayers.

Structure	The Length of Bond (Å)		Bond Angle (°)		Adsorption Distance (Å)	Atom	Mulliken Charge (e)	Q_t (e)	Ead (eV)
Pd-InP_3/SO_2	S-O_1	1.563	O_1-S-O_2	113.199	2.430	S	0.427	−0.420	−1.635
						O_1	−0.398		
	S-O_2	1.564				O_2	−0.449		
Pt-InP_3/SO_2	S-O_1	1.556	O_1-S-O_2	111.696	2.403	S	0.416	−0.438	−1.822
						O_1	−0.414		
	S-O_2	1.576				O_2	−0.440		
Au-InP_3/SO_2	S-O_1	1.486	O_1-S-O_2	114.541	4.209	S	0.372	−0.341	−1.033
						O_1	−0.284		
	S-O_2	1.558				O_2	−0.429		
Fe-InP_3/SO_2	S-O_1	1.624	O_1-S-O_2	113.729	2.059	S	0.404	−0.483	−2.276
						O_1	−0.437		
	S-O_2	1.573				O_2	−0.450		
Co-InP_3/SO_2	S-O_1	1.620	O_1-S-O_2	114.341	2.170	S	0.451	−0.448	−2.019
						O_1	−0.447		
	S-O_2	1.566				O_2	−0.452		
Mo-InP_3/SO_2	S-O_1	1.638	O_1-S-O_2	110.233	2.123	S	0.361	−0.539	−2.800
						O_1	−0.444		
	S-O_2	1.583				O_2	−0.456		

Table 3. Parameters of SO_2 adsorption by intrinsic InP_3 monolayer.

	E_{ad} (eV)	Q_t (e)
InP_3/SO_2	−1.050	−0.545

By analyzing the experimental data, it was found that the E_{ad} of the adsorption model with the largest absolute value in the Au-InP_3/SO_2 system was −1.033 eV, which is close to the E_{ad} of the InP_3/SO_2 system in Table 3 (E_{ad} = −1.050 eV). The adsorption model in Figure 4c was observed, and it was found that the SO_2 molecule was far away from the Au dopant but close to a P atom on the InP_3 monolayer. It is speculated that the Au dopant has no significant effect on the adsorption of SO_2 by the InP_3 monolayer. In the above five adsorption systems (except for the Au-InP_3/SO_2 system), the adsorption energy ranged from −1.635 eV to −2.800 eV, which are markedly improved compared with the adsorption energy of SO_2 using the intrinsic InP_3 monolayer. The range of Q_t was −0.420 e to −0.539 e. The adsorption effect was ranked as Mo-InP_3/SO_2 > Fe-InP_3/SO_2 > Co-InP_3/SO_2 > Pt-InP_3/SO_2 > Pd-InP_3/SO_2. The above data show that the adsorption processes of the five TM-InP_3/SO_2 systems are all chemical adsorption, and negative Q_t means that SO_2 molecules act as electron acceptors and accept the electron transferred from TM-InP_3 monolayers. After the adsorption process, the S-O bonds of SO_2 molecules in five systems (except for the Au-InP_3/SO_2 system) are lengthened to different degrees, and the O-S-O bond angles are decreased to different degrees. It can be observed in Figure 4 that TM-InP_3 monolayers with adsorbed SO_2 have pronounced geometric deformation. In particular, as can be seen from Figure 4e, the position of Co has moved considerably, and

the Co-In bond has been extended from 2.615 Å to 2.920 Å after adsorption. The Co atom has captured the SO_2 molecule through the S atom. The adsorption distance is 2.170 Å, and it is presumed that a Co-S bond with the same length is formed between them. Similarly, in the InP_3 monolayer system with Pd, Pt, Fe and Mo as dopants, SO_2 molecules were captured by doped atoms, forming a Pd-S bond of 2.430 Å, a Pt-S bond of 2.403 Å, an Fe-S bond of 2.059 Å and a Mo-S bond of 2.123 Å, respectively. Through the above analysis, it is speculated that it is precisely because of the good catalytic properties of Pd, Pt, Fe, Co and Mo atoms that SO_2 molecules are activated in the adsorption process.

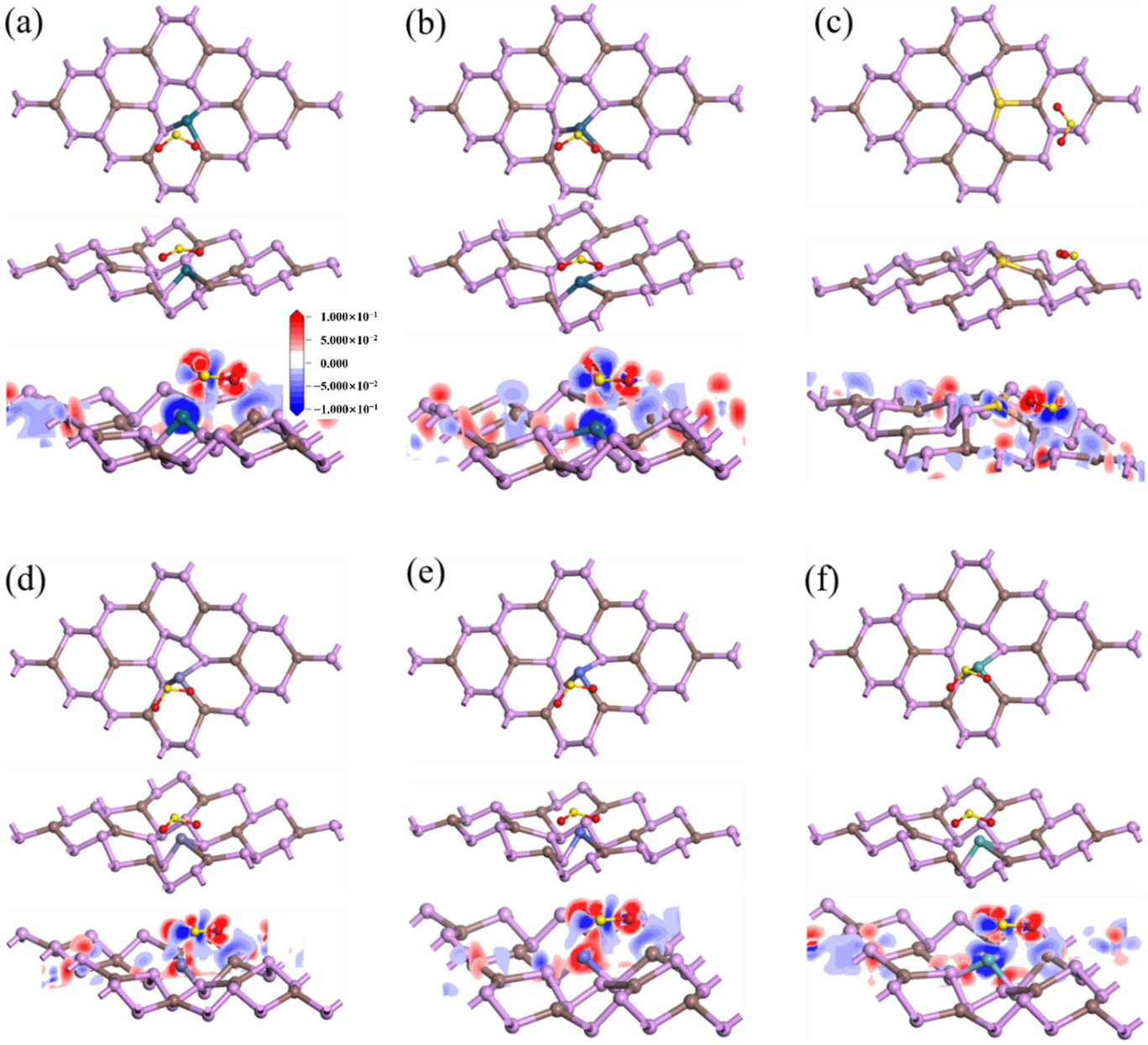

Figure 4. Adsorptive structure and DCD of (**a**) Pd-InP_3/SO_2, (**b**) Pt-InP_3/SO_2, (**c**) Au-InP_3/SO_2, (**d**) Fe-InP_3/SO_2, (**e**) Co-InP_3/SO_2 and (**f**) Mo-InP_3/SO_2.

Next, the interactions between SO_2 and TM-InP_3 monolayers were further verified by DCD. In Pd-InP_3, Pt-InP_3 and Mo-InP_3 adsorption systems, the electron depletion regions are mainly concentrated on TM-doped atoms, while in Fe-InP_3 and Co-InP_3 adsorption systems, the electron aggregation areas are around TM dopants. From the DCD diagrams of the above five systems, we can see that there is a pronounced overlap between the

electron depletion regions and the electron aggregation regions, which means that there are strong interactions between SO_2 and TM-InP_3 and the formation of new chemical bonds. However, for the Au-InP_3 adsorption system, there is no apparent continuous electron region between Au and SO_2 molecules, which implies that there is no significant charge transfer and no stable chemical bond formation between the SO_2 molecule and Au.

The DOS of the adsorption systems was analyzed to further explore the electronic behaviors of SO_2 molecules adsorbed by TM-InP_3 monolayers. It can be seen in Figure 5 that in Pd-InP_3, Pt-InP_3, Fe-InP_3 and Mo-InP_3 systems, after SO_2 was adsorbed, the TDOS of the systems moved considerably to the right, which means that the conductivity of the systems decreased. However, the TDOS of Au-InP_3 and Co-InP_3 systems did not show notable displacement, and the conductivity of the systems changed little after gas adsorption. Before and after SO_2 adsorption, the α-spin and β-spin of Fe-InP_3 and Mo-InP_3 monolayers were highly asymmetric near the Fermi level, which indicates that the two systems that adsorbed SO_2 still had magnetism. In all TM-InP_3/SO_2 systems, a number of new peaks appeared between −6 eV and −8 eV, which are attributed to SO_2 after its adsorption. The appearance of a new peak means that SO_2 molecules are activated by TM-InP_3 monolayers, and it is speculated that this is mainly caused by orbital hybridization between TM atoms and SO_2.

Therefore, the PDOSs of the six systems were thoroughly analyzed. Taking the Pd-InP_3/SO_2 system as an example, Pd-4d, S-2p and O-2p orbitals markedly overlap between −8 eV and 2 eV, so there is an intense hybridization phenomenon between them, which contributes to the formation of stable chemical bonds. This confirms our previous assumption. Similarly, in Pt-InP_3/SO_2, Fe-InP_3/SO_2, Co-InP_3/SO_2 and Mo-InP_3/SO_2 systems, the atomic orbits of TM atoms overlap with those of SO_2 in a large range, and the orbitals of SO_2 and TM atoms are highly hybridized. For the Au-InP_3/SO_2 system, we found that the Au-5d, S-3p and O-2p orbitals only slightly overlap from −4 eV to −2 eV, so it is speculated that there is no stable chemical bond between SO_2 molecules and Au atoms. Combined with the previous discussion, it can be inferred that using Au as the dopant does not enhance the adsorption properties of the InP_3 monolayer for SO_2, and its adsorption effect is similar to that of the intrinsic InP_3 monolayer. These phenomena indicate that, apart from the Au-InP_3/SO_2 system, there are new bonds between SO_2 and TM atoms, which gives SO_2 excellent chemisorption effects on TM-InP_3 monolayers and greatly affects the electronic behavior of intrinsic materials. In other words, the doping of five kinds of TM atoms (except for Au atoms) provides InP_3 monolayers with better adsorption stability for SO_2.

3.4. Frontier Orbital Theory and Gas Sensing Mechanism Analysis

The change in conductivity in TM-InP_3 monolayers caused by SO_2 adsorption was further studied, and the possibility of using them as SO_2 resistive sensing materials was explored. On the basis of frontier molecular orbital (FMO) theory, the LUMO and HOMO of the systems were calculated, and the energy between them is the band gap. From the previous analysis of the energy band diagram, it is known that a wider band gap means that it has lower conductivity. It can be found in Figure 6 that the LUMO and HOMO of TM (Pd, Pt, Fe, Co and Mo)-InP_3 systems after gas adsorption changed compared with those before gas adsorption, which implies that the gas adsorption process redistributes the electrons of the system. However, for the Au-InP_3 system, HOMO and LUMO did not markedly change before and after adsorption, which means that the adsorption process had little effect on the electronic behavior of the material. This shows again that the doping of Au did not improve the adsorption effect of SO_2, which is consistent with the previous conclusion. In the six TM-InP_3 systems, the adsorption of SO_2 changed the conductivity of the InP_3 monolayer to different degrees. For Pd-InP_3 and Pt-InP_3 monolayers, after adsorption, their band gaps increased to 0.330 eV and 0.148 eV, respectively, and their conductivity decreased. The adsorption of SO_2 made the two monolayers behave as semiconductors [57]. Both of them are potential choices as SO_2 sensor materials. For the Au-InP_3 monolayer, its band gap only

increased by 0.022 eV. Combined with previous research on its adsorption performance, it is concluded that it is not a suitable SO_2 sensor. Similarly, for the Co-InP_3 monolayer, although it has an excellent adsorption effect on SO_2, its energy band changed little, only increasing by 0.024 eV, so it is not suitable as a material for detecting SO_2. However, for Fe-InP_3 and Mo-InP_3 monolayers, the absorption of SO_2 made their band gaps almost double, so the conductivity decreased significantly. This provides us with two potential choices for the research of ideal SO_2 resistive sensor materials.

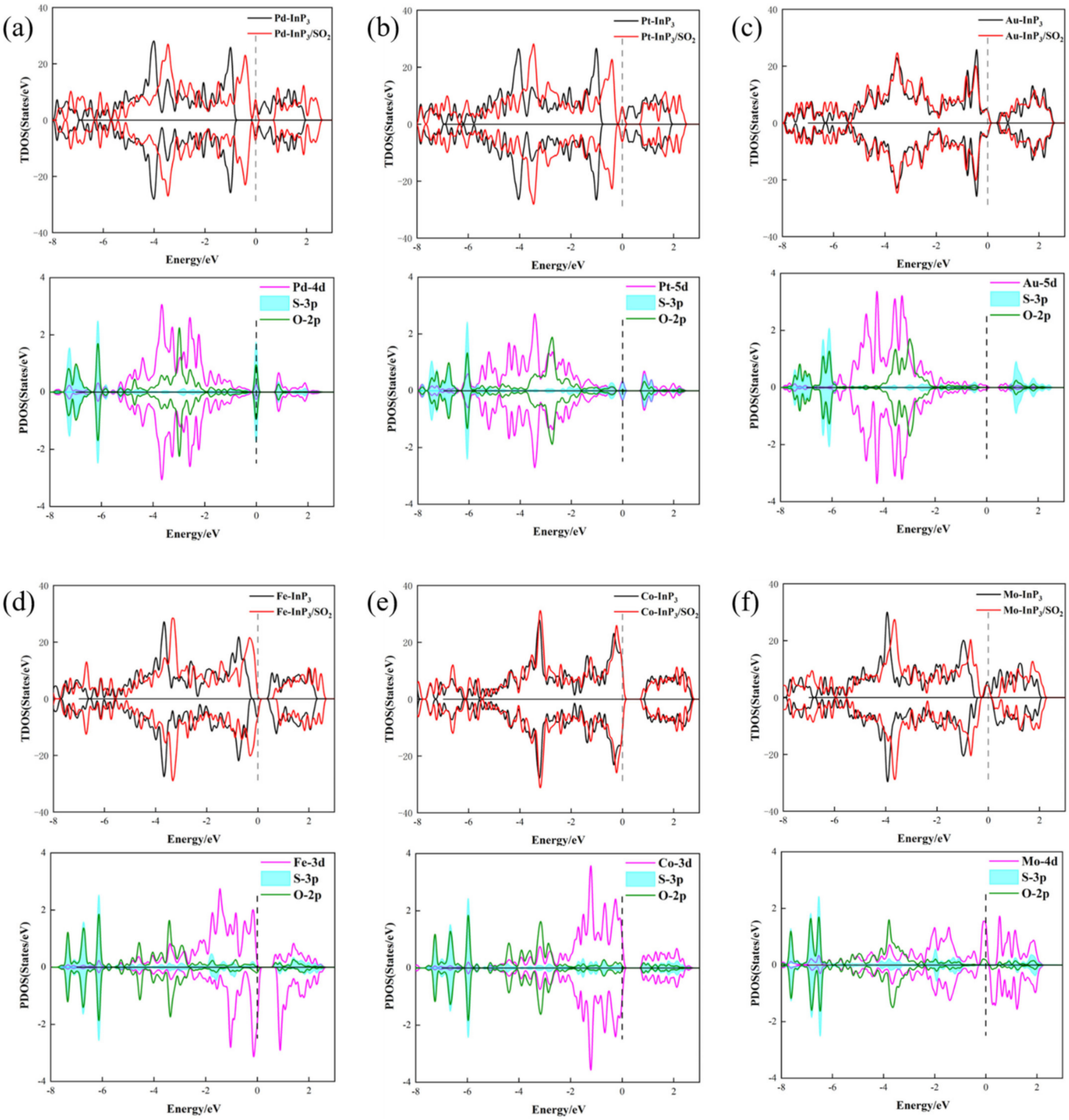

Figure 5. DOS of (**a**) Pd-InP_3/SO_2, (**b**) Pt-InP_3/SO_2, (**c**) Au-InP_3/SO_2, (**d**) Fe-InP_3/SO_2, (**e**) Co-InP_3/SO_2 and (**f**) Mo-InP_3/SO_2.

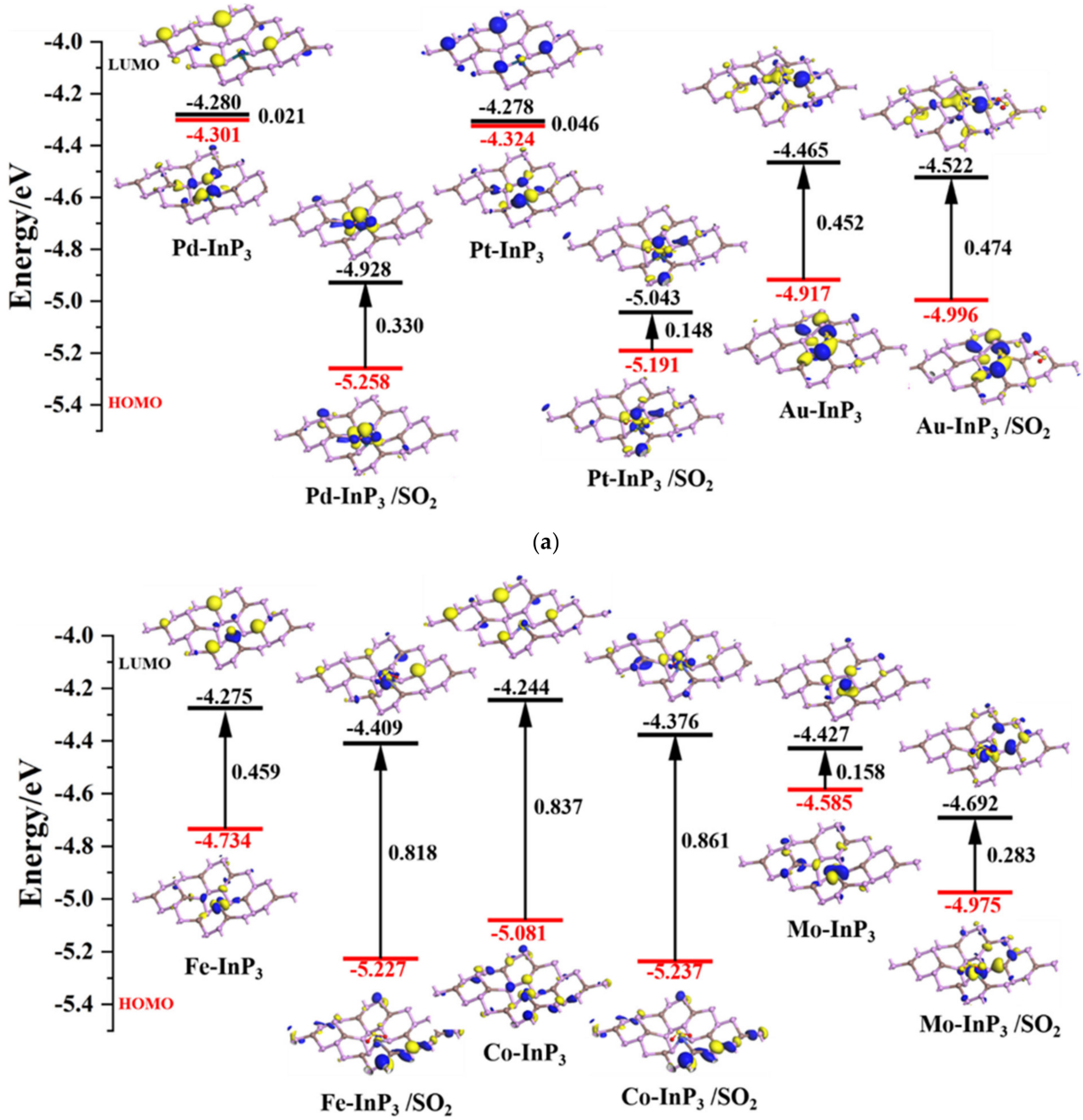

Figure 6. HOMO and LUMO distributions of TM-InP_3 monolayers and TM-InP_3/SO_2 systems, (**a**) TM = Pd, Pt, Au, (**b**) TM = Fe, Co, Mo.

3.5. Recovery Time Analysis

Recovery time refers to the time required for gas to desorb from the adsorption material, and it is an essential index for judging the gas sensing performance of the material. It is calculated by the following formula:

$$\tau = A^{-1}e^{(-E_a/K_BT)} \quad (4)$$

where a is the attempt frequency, which is a constant with a value of 10^{12} s^{-1} [58,59]. K_B is the Boltzmann constant (8.62×10^{-5} eV/K), and T is the ambient temperature. E_a represents the energy barrier to be overcome in the desorption process, which is often displaced by E_{ad}. The desorption time of SO_2 on the six kinds of adsorption materials at three different temperatures (298 K, 498 K and 698 K) was calculated and is shown in

Figure 7. At room temperature (298 K), the desorption time of SO_2 on Au-InP_3 was the shortest. For Pd-InP_3, Pt-InP_3, Co-InP_3 and Fe-InP_3 monolayers, the desorption time of SO_2 at room temperature was very long, but the recovery time was significantly shortened when the temperature rose to 698 K. Their minimum value was only 0.63 s (Pd-InP_3), and the recovery time of the maximum Fe-InP_3 was 7.4 h. They had stable adsorption performance for SO_2 at room temperature and a short recovery time at high temperature, which means that they can be used as gas sensors many times and recycled. For the Mo-InP_3 monolayer, even at the high temperature of 698 K, it still took about 5 years for SO_2 to be released from the material surface. This means that the Mo-InP_3 monolayer has a strong ability to remove SO_2. Therefore, the Mo-InP_3 monolayer can be developed into a disposable SO_2 resistance sensor with a scavenger function, which can detect and remove SO_2.

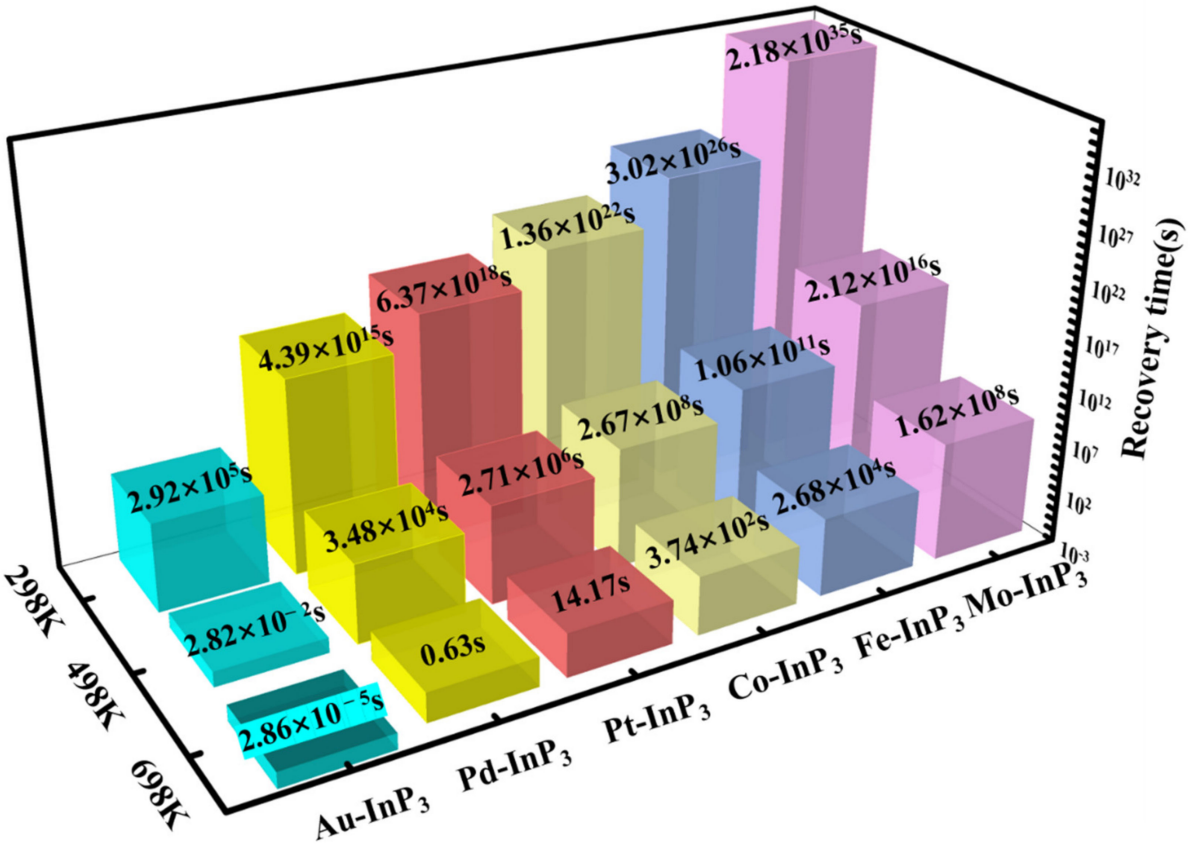

Figure 7. Recovery time of TM-InP_3 monolayers toward SO_2.

4. Conclusions

All of the research in this paper is based on the first-principles theory. The effects of TM (Pd, Pt, Au, Fe, Co and Mo) dopants on the configuration and electronic behavior of InP_3 monolayers were studied. Through the analysis of DCD, DOS and frontier orbital theory, the adsorption characteristics, electronic behavior and sensing mechanism of SO_2 on TM-InP_3 monolayers were explored. The main conclusions are as follows:

1. Pd, Pt, Fe, Co and Mo atoms are more inclined to replace the P atom at the P_1 site in the InP_3 monolayer, while Au atoms are more inclined to replace the P_2 atom. Orbital hybridization makes the dopant form stable TM-P bonds and TM-In bonds with the intrinsic InP_3 monolayer.
2. The adsorption of SO_2 on TM-InP_3 monolayers was characterized as chemical adsorption, and SO_2 showed electron acceptance behavior.
3. Combined with the analysis of E_{ad} and Q_t of six adsorption systems, the adsorption effect of TM-InP_3 monolayers for SO_2 was in the following order: Mo-InP_3 > Fe-InP_3

> Co-InP_3 > Pt-InP_3 > Pd-InP_3 > Au-InP_3. Except for the Au atom, the other five TM atoms as InP_3 dopants significantly enhanced the adsorption effect of the InP_3 monolayer for SO_2, and considerable orbital hybridization and stable chemical bonds were formed between dopants and SO_2.

4. The adsorption of SO_2 resulted in a change in the conductivity of TM-InP_3 monolayers to different degrees. Combined with the adsorption effect of the six systems for SO_2, this shows that Pd-InP_3, Pt-InP_3, Fe-InP_3 and Mo-InP_3 monolayers have great potential to be used as resistive SO_2 sensors, among which Fe-InP_3 and Mo-InP_3 are the most promising SO_2 sensor candidates.

Author Contributions: Conceptualization, T.H.; methodology, T.H. and Q.Z.; validation, T.H.; investigation, T.H.; data curation, T.H.; writing—original draft, T.H.; writing—review and editing, T.H., Q.Z. and W.Z.; supervision, Q.Z.; project administration, Q.Z. All authors have read and agreed to the published version of the manuscript.

Funding: This study has been supported in part by the National Natural Science Foundation of China (Nos. 52077177 and 51507144) and Fundamental Research Funds for the Central Universities (No. XDJK2019B021).

Data Availability Statement: The data are available on request from the corresponding author.

Conflicts of Interest: The authors declare no conflict of interest.

References

1. Chen, W.T.; Yan, W.T. Impact of internet electronic commerce on SO_2 pollution: Evidence from China. *Environ. Sci. Pollut. Res.* **2020**, *27*, 25801–25812. [CrossRef] [PubMed]
2. Salih, E.; Ayesh, A.I. Sensitive SO_2 gas sensor utilizing Pt-doped graphene nanoribbon: First principles investigation. *Mater. Chem. Phys.* **2021**, *267*, 124695. [CrossRef]
3. Meng, W.; Zeng, B.; Huang, H. Forecasting of Sulfur Dioxide Emissions in China Based on Optimized DGM(1,1). In Proceedings of the IEEE International Conference on Grey Systems and Intelligent Services (GSIS), Stockholm, Sweden, 8–11 August 2017; pp. 159–164.
4. Shao, L.; Chen, G.D.; Ye, H.G.; Niu, H.B.; Wu, Y.L.; Zhu, Y.Z.; Ding, B.J. Sulfur dioxide molecule sensors based on zigzag graphene nanoribbons with and without Cr dopant. *Phys. Lett. A* **2014**, *378*, 667–671. [CrossRef]
5. Linn, W.S.; Avol, E.L.; Peng, R.C.; Shamoo, D.A.; Hackney, J.D. Replicated dose-response study of sulfur dioxide effects in normal, atopic, and asthmatic volunteers. *Am. Rev. Respir. Dis.* **1987**, *136*, 1127–1134. [CrossRef]
6. Noei, M. Different electronic sensitivity of BN and AlN nanoclusters to SO_2 gas: DFT studies. *Vacuum* **2017**, *135*, 44–49. [CrossRef]
7. Sun, Y.L.; Jiang, Q.; Wang, Z.F.; Fu, P.Q.; Li, J.; Yang, T.; Yin, Y. Investigation of the sources and evolution processes of severe haze pollution in Beijing in January 2013. *J. Geophys. Res. Atmos.* **2014**, *119*, 4380–4398. [CrossRef]
8. Xie, Y.; Dai, H.C.; Zhang, Y.X.; Wu, Y.Z.; Hanaoka, T.; Masui, T. Comparison of health and economic impacts of $PM_{2.5}$ and ozone pollution in China. *Environ. Int.* **2019**, *130*, 104881. [CrossRef]
9. Ye, X.; Jiang, X.; Chen, L.; Jiang, W.J.; Wang, H.L.; Cen, W.L.; Ma, S.G. Effect of manganese dioxide crystal structure on adsorption of SO_2 by DFT and experimental study. *Appl. Surf. Sci.* **2020**, *521*, 146477. [CrossRef]
10. Zhang, X.X.; Dai, Z.Q.; Chen, Q.C.; Tang, J. A DFT study of SO_2 and H_2S gas adsorption on Au-doped single-walled carbon nanotubes. *Phys. Scr.* **2014**, *89*, 065803. [CrossRef]
11. Zhou, J.H.; Gou, X.T.; Shi, Z.T.; Lian, Y.; Zhao, J.G.; Li, P. Thinking and Suggestion on Promoting the Trade of SO_2 Pollution Right. In Proceedings of the International Conference on Innovation Managements, Wuhan, China, 8–9 December 2009; pp. 40–42.
12. Alsiraji, H.A. Assessment of Graphene Band Gap Based on Varying the Interaction Energy Coefficients. In Proceedings of the IEEE Jordan International Joint Conference on Electrical Engineering and Information Technology (JEEIT), Amman, Jordan, 9–11 April 2019; pp. 878–882.
13. Yu, Z.G.; Zhang, Y.W. Band gap engineering of graphene with inter-layer embedded BN: From first principles calculations. *Diam. Relat. Mater.* **2015**, *54*, 103–108. [CrossRef]
14. Li, Z.H.; Jia, L.F.; Chen, J.X.; Cui, X.S.; Zeng, W.; Zhou, Q. Ag-modified hexagonal GaN monolayer as an innovative gas detector toward SF_6 decomposed species: Insights from the first-principles computations. *Appl. Surf. Sci.* **2022**, *589*, 153000. [CrossRef]
15. Qian, G.C.; Dai, W.J.; Zhou, F.R.; Ma, H.M.; Wang, S.; Hu, J.; Zhou, Q. Adsorption Characteristics of Carbon Monoxide on Ag- and Au-Doped HfS_2 Monolayers Based on Density Functional Theory. *Chemosensors* **2022**, *10*, 82. [CrossRef]
16. Chen, G.X.; Wang, R.X.; Li, H.X.; Chen, X.N.; An, G.; Zhang, J.M. First-principles study of pristine and metal decorated blue phosphorene for sensing toxic H_2S, SO_2 and NO_2 molecules. *Appl. Phys. A-Mater. Sci. Process.* **2021**, *127*, 133. [CrossRef]
17. Mi, H.W.; Zhou, Q.; Zeng, W. A density functional theory study of the adsorption of Cl_2, NH_3, and NO_2 on Ag_3-doped WSe_2 monolayers. *Appl. Surf. Sci.* **2021**, *563*, 150329. [CrossRef]

18. Abbas, A.N.; Liu, B.L.; Chen, L.; Ma, Y.Q.; Cong, S.; Aroonyadet, N.; Kopf, M.; Nilges, T.; Zhou, C.W. Black Phosphorus Gas Sensors. *ACS Nano* **2015**, *9*, 5618–5624. [CrossRef]
19. Li, L.K.; Yu, Y.J.; Ye, G.J.; Ge, Q.Q.; Ou, X.D.; Wu, H.; Feng, D.L.; Chen, X.H.; Zhang, Y.B. Black phosphorus field-effect transistors. *Nat. Nanotechnol.* **2014**, *9*, 372–377. [CrossRef]
20. Dos Santos, R.B.; Rivelino, R.; Gueorguiev, G.K.; Kakanakova-Georgieva, A. Exploring 2D structures of indium oxide of different stoichiometry. *Crystengcomm* **2021**, *23*, 6661–6667. [CrossRef]
21. Kakanakova-Georgieva, A.; Giannazzo, F.; Nicotra, G.; Cora, I.; Gueorguiev, G.K.; Persson, P.O.A.; Pecz, B. Material proposal for 2D indium oxide. *Appl. Surf. Sci.* **2021**, *548*, 149275. [CrossRef]
22. Ouyang, T.; Jiang, E.L.; Tang, C.; Li, J.; He, C.Y.; Zhong, J.X. Thermal and thermoelectric properties of monolayer indium triphosphide (InP_3): A first-principles study. *J. Mater. Chem. A* **2018**, *6*, 21532–21541. [CrossRef]
23. Zhang, M.; Guo, H.M.; Lv, J.; Jia, J.F.; Wu, H.S. The 3d transition-metals doping tunes the electronic and magnetic properties of 2D monolayer InP_3. *J. Magn. Magn. Mater.* **2021**, *533*, 168028. [CrossRef]
24. Yang, H.R.; Wang, Z.P.; Ye, H.Y.; Zhang, K.; Chen, X.P.; Zhang, G.Q. Promoting sensitivity and selectivity of HCHO sensor based on strained InP_3 monolayer: A DFT study. *Appl. Surf. Sci.* **2018**, *459*, 554–561. [CrossRef]
25. Jalil, A.; Zhuo, Z.W.; Sun, Z.T.; Wu, F.; Wang, C.; Wu, X.J. A phosphorene-like InP_3 monolayer: Structure, stability, and catalytic properties toward the hydrogen evolution reaction. *J. Mater. Chem. A* **2020**, *8*, 1307–1314. [CrossRef]
26. Wu, W.X.; Zhang, Y.M.; Guo, Y.H.; Bai, J.X.; Zhang, C.H.; Chen, Z.F.; Liu, Y.X.; Xiao, B.B. Exploring anchoring performance of InP_3 monolayer for lithium-sulfur batteries: A first-principles study. *Appl. Surf. Sci.* **2020**, *526*, 146717. [CrossRef]
27. Miao, N.H.; Xu, B.; Bristowe, N.C.; Zhou, J.; Sun, Z.M. Tunable Magnetism and Extraordinary Sunlight Absorbance in Indium Triphosphide Monolayer. *J. Am. Chem. Soc.* **2017**, *139*, 11125–11131. [CrossRef]
28. Yi, W.C.; Chen, X.; Wang, Z.X.; Ding, Y.C.; Yang, B.C.; Liu, X.B. A novel two-dimensional delta-InP_3 monolayer with high stability, tunable bandgap, high carrier mobility, and gas sensing of NO_2. *J. Mater. Chem. C* **2019**, *7*, 7352–7359. [CrossRef]
29. Liao, Y.M.; Zhou, Q.; Hou, W.J.; Li, J.; Zeng, W. Theoretical study of dissolved gas molecules in transformer oil adsorbed on intrinsic and Cr-doped InP_3 monolayer. *Appl. Surf. Sci.* **2021**, *561*, 149816. [CrossRef]
30. Cui, H.; Jia, P.F. Doping effect of small Rh-n (n = 1–4) clusters on the geometric and electronic behaviors of MoS_2 monolayer: A first-principles study. *Appl. Surf. Sci.* **2020**, *526*, 146659. [CrossRef]
31. Li, B.L.; Zhou, Q.; Peng, R.C.; Liao, Y.M.; Zeng, W. Adsorption of SF_6 decomposition gases (H_2S, SO_2, SOF_2 and SO_2F_2) on Sc-doped MoS_2 surface: A DFT study. *Appl. Surf. Sci.* **2021**, *549*, 149271. [CrossRef]
32. Peng, R.C.; Zhou, Q.; Zeng, W. First-Principles Study of Au-Doped InN Monolayer as Adsorbent and Gas Sensing Material for SF_6 Decomposed Species. *Nanomaterials* **2021**, *11*, 1708. [CrossRef]
33. Peng, R.C.; Zhou, Q.; Zeng, W. First-Principles Insight into Pd-Doped C_3N Monolayer as a Promising Scavenger for NO, NO_2 and SO_2. *Nanomaterials* **2021**, *11*, 1267. [CrossRef]
34. Lu, Z.; Zhai, Y.; Liang, Q.Z.; Wu, W. Research paper Promoting sensitivity and selectivity of NO_2 gas sensor based on metal (Pt, Re, Ta)-doped monolayer WSe_2: A DFT study. *Chem. Phys. Lett.* **2020**, *755*, 137737. [CrossRef]
35. Chen, D.C.; Zhang, X.X.; Tang, J.; Cui, H.; Li, Y. Noble metal (Pt or Au)-doped monolayer MoS_2 as a promising adsorbent and gas-sensing material to SO_2, SOF_2 and SO_2F_2: A DFT study. *Appl. Phys. A-Mater. Sci. Process.* **2018**, *124*, 194. [CrossRef]
36. Zhang, H.P.; Luo, X.G.; Song, H.T.; Lin, X.Y.; Lu, X.; Tang, Y.H. DFT study of adsorption and dissociation behavior of H_2S on Fe-doped graphene. *Appl. Surf. Sci.* **2014**, *317*, 511–516. [CrossRef]
37. Xie, T.Y.; Wang, P.; Tian, C.F.; Zhao, G.Z.; Jia, J.F.; Zhao, C.X.; Wu, H.S. The Adsorption Behavior of Gas Molecules on Co/N Co-Doped Graphene. *Molecules* **2021**, *26*, 7700. [CrossRef]
38. Tabtimsai, C.; Wanno, B.; Utairueng, A.; Promchamorn, P.; Kumsuwan, U. First Principles Investigation of NH_3 and NO_2 Adsorption on Transition Metal-Doped Single-Walled Carbon Nanotubes. *J. Electron. Mater.* **2019**, *48*, 7226–7238. [CrossRef]
39. Delley, B. From molecules to solids with the $DMol^3$ approach. *J. Chem. Phys.* **2000**, *113*, 7756–7764. [CrossRef]
40. Perdew, J.P.; Burke, K.; Ernzerhof, M. Generalized Gradient Approximation Made Simple. *Phys. Rev. Lett.* **1996**, *77*, 3865. [CrossRef]
41. Tkatchenko, A.; DiStasio, R.A.; Head-Gordon, M.; Scheffler, M. Dispersion-corrected Moller-Plesset second-order perturbation theory. *J. Chem. Phys.* **2009**, *131*, 094106. [CrossRef]
42. Delley, B. Hardness conserving semilocal pseudopotentials. *Phys. Rev. B* **2002**, *66*, 155125. [CrossRef]
43. Liao, Y.M.; Zhou, Q.; Peng, R.C.; Zeng, W. Adsorption properties of InP_3 monolayer toward SF_6 decomposed gases: A DFT study. *Phys. E* **2021**, *130*, 114689. [CrossRef]
44. Jiang, T.Y.; Zhang, T.; He, Q.Q.; Bi, M.Q.; Chen, X.; Zhou, X. Adsorption performance and gas-sensing properties of V-GaSe to SF_6 decomposition components in gas-insulated switchgear. *Appl. Surf. Sci.* **2022**, *577*, 151854. [CrossRef]
45. Mom, R.V.; Cheng, J.; Koper, M.T.M.; Sprik, M. Modeling the Oxygen Evolution Reaction on Metal Oxides: The Infuence of Unrestricted DFT Calculations. *J. Phys. Chem. C* **2014**, *118*, 4095–4102. [CrossRef]
46. Liu, Y.P.; Zhou, Q.; Hou, W.J.; Li, J.; Zeng, W. Adsorption properties of Cr modified GaN monolayer for H_2, CO, C_2H_2 and C_2H_4. *Chem. Phys.* **2021**, *550*, 111304. [CrossRef]
47. Gao, X.; Zhou, Q.; Wang, J.X.; Xu, L.N.; Zeng, W. Adsorption of SO_2 molecule on Ni-doped and Pd-doped graphene based on first-principle study. *Appl. Surf. Sci.* **2020**, *517*, 146180. [CrossRef]

48. Liu, Y.P.; Zhou, Q.; Wang, J.X.; Zeng, W. Cr doped MN (M = In, Ga) monolayer: A promising candidate to detect and scavenge SF_6 decomposition components. *Sens. Actuators A Phys.* **2021**, *330*, 112854. [CrossRef]
49. Zeng, F.P.; Feng, X.X.; Chen, X.Y.; Yao, Q.; Miao, Y.L.; Dai, L.J.; Li, Y.; Tang, J. First-principles analysis of $Ti_3C_2T_x$ MXene as a promising candidate for SF_6 decomposition characteristic components sensor. *Appl. Surf. Sci.* **2022**, *578*, 152020. [CrossRef]
50. Zhang, X.X.; Gui, Y.G.; Dai, Z.Q. A simulation of Pd-doped SWCNTs used to detect SF_6 decomposition components under partial discharge. *Appl. Surf. Sci.* **2014**, *315*, 196–202. [CrossRef]
51. Cui, H.; Zhang, X.X.; Zhang, G.Z.; Tang, J. Pd-doped MoS_2 monolayer: A promising candidate for DGA in transformer oil based on DFT method. *Appl. Surf. Sci.* **2019**, *470*, 1035–1042. [CrossRef]
52. Wang, J.X.; Zhou, Q.; Zeng, W. Competitive adsorption of SF_6 decompositions on Ni-doped ZnO (100) surface: Computational and experimental study. *Appl. Surf. Sci.* **2019**, *479*, 185–197. [CrossRef]
53. Gong, P.L.; Zhang, F.; Huang, L.F.; Zhang, H.; Li, L.; Xiao, R.C.; Deng, B.; Pan, H.; Shi, X.Q. Multifunctional two-dimensional semiconductors SnP3: Universal mechanism of layer-dependent electronic phase transition. *J. Phys. Condens. Matter* **2018**, *30*, 475702. [CrossRef]
54. Ghosh, B.; Puri, S.; Agarwal, A.; Bhowmick, S. SnP3: A Previously Unexplored Two-Dimensional Material. *J. Phys. Chem. C* **2018**, *122*, 18185–18191. [CrossRef]
55. Sun, S.S.; Meng, F.C.; Wang, H.Y.; Wang, H.; Ni, Y.X. Novel two-dimensional semiconductor SnP3: High stability, tunable bandgaps and high carrier mobility explored using first-principles calculations. *J. Mater. Chem. A* **2018**, *6*, 11890–11897. [CrossRef]
56. Haase, J. Structural studies of SO_2 adsorption on metal surfaces. *J. Phys. Condens. Matter.* **1997**, *9*, 1647–1670. [CrossRef]
57. Liu, Y.; Shi, T.; Si, Q.L.; Liu, T. Adsorption and sensing performances of transition metal (Pd, Pt, Ag and Au) doped $MoTe_2$ monolayer upon NO_2: A DFT study. *Phys. Lett. A* **2021**, *391*, 127117. [CrossRef]
58. Lee, J.M.; Lim, S.H. Thermally activated magnetization switching in a nanostructured synthetic ferrimagnet. *J. Appl. Phys.* **2013**, *113*, 063914.
59. Boerner, E.D.; Bertram, H.N. Non-Arrhenius behavior in single domain particles. *IEEE Trans. Magn.* **1998**, *34*, 1678–1680. [CrossRef]